Optical properties of Fe-based semimagnetic semiconductors

1990 J. Phys.: Condens. Matter 2 8173

(http://iopscience.iop.org/0953-8984/2/41/005)

J. Phys.: Condens. Matter 2 (1990) 8173–8187. Printed in the UK

Optical properties of Fe-based semimagnetic semiconductors

A Sarem†, B J Kowalski and B A Orłowski
Institute of Physics, Polish Academy of Sciences, Al. Lotników 32/46, 02-688 Warszawa, Poland

Received 5 February 1990, in final form 12 June 1990

Abstract. The reflectivity spectra of $Hg_{1-x}Fe_xSe$ ($0 \leq x \leq 0.15$), $Cd_{1-x}Fe_xSe$ ($0 \leq x \leq 0.12$) and $Cd_{1-x}Fe_xTe$ ($0 \leq x \leq 0.06$) crystals have been investigated in the 1–12 eV energy range. The observed changes in the shapes of the spectra, caused by the increase in the Fe content, have been compared with the calculated band structure of binary compounds available in the literature. The band structure in some regions seems to be sensitive to the presence of Fe ions. Most of the structures of the spectra are broadened owing to structural, chemical and magnetic disorder occurring in the lattice due to the Fe contribution. The results obtained contribute to the model of the electronic structure of these compounds proposed in the literature.

1. Introduction

The term 'semimagnetic semiconductor' (SMSC) or 'diluted magnetic semiconductor' applies to any semiconducting material, which is partially made up of magnetic atoms (i.e. II–VI, II–V or IV–VI materials with magnetic ions) [1–5]. Their properties (electrical, optical and magnetic) are strongly modified by the s–p–d exchange interaction between the localised d electrons of the transition-metal magnetic ions and the mobile carriers in the conduction or the valence band [4, 5]. These materials show characteristics that are interesting from the point of view of applications in infrared detectors, lasers and other optical devices [2, 5].

The most thoroughly studied groups of SMSCs are the II–VI compounds containing substitutional Mn^{2+}, Fe^{2+} and recently Co^{2+} [5–7]. Among these, the group of Mn-based SMSCs has been investigated widely and for a long time. SMSCs of this group exhibit unique properties since the solubility of the magnetic component can be controlled in a very wide range (from doped to mixed crystals; up to $x = 0.7$) [5].

In comparison with Mn, an Fe atom possesses one more electron. So, the Fe $3d^6$ state is located above the Mn $3d^5$ state in a semiconductor band structure [6]. Therefore, the SMSCs containing substitutional Fe^{2+} ions have been extensively studied recently, because of their interesting magneto-optical and magnetic properties [6, 8]. The magnetic elements occupy the lattice sites of the group II atoms in the hosts. The magnetic properties of Fe-based SMSCs are determined by the Fe–Fe exchange interaction at both

† Permanent address: Department of Physics, Faculty of Science, Tishreen University, Lattakia, Syria.

0953-8984/90/418173 + 15 $03.50

low and high temperatures [9, 10]. At low temperatures, for low values of x, the Van Vleck susceptibility was observed (not only for $Hg_{1-x}Fe_xSe$) and the SMSC behaves like a paramagnetic substance, while in more concentrated samples ($x \geq 0.1$), a spin-glass phase was found. At high temperatures, the exchange interaction between the nearest-neighbour Fe^{2+} ions is antiferromagnetic for all values of x [10–12]. Therefore, these materials may be viewed as SMSCs.

The best-known SMSCs of $A^{II}_{1-x}Fe_xB^{VI}$ type are narrow-gap $Hg_{1-x}Fe_xSe$ and wide-gap $Cd_{1-x}Fe_xSe$ and $Cd_{1-x}Fe_xTe$. A characteristic feature of these materials is that the location of the Fe^{2+} $3d^6$ state is either in the forbidden band gap, as a deep donor state ($Cd_{1-x}Fe_xSe$ and $Cd_{1-x}Fe_xTe$), or in the conduction band as a resonant donor state ($Hg_{1-x}Fe_xSe$) [6, 8, 13]. Figure 1 illustrates the location of the Fe donor state in the band structure of these alloys, with the band extrema occurring at the centre of the Brillouin zone (BZ) ($\boldsymbol{k} = \mathbf{0}$). At low concentrations, the Fe ions act as impurities in the band gap, causing the pinning of the Fermi level. With an increase in the Fe content up to the ternary alloy region, the position of the Fe $3d^6$ level will correspond to the valence band edge of the alloy [7, 14].

The lattice constants of $Cd_{1-x}Fe_xSe$ up to $x = 0.12$ [15], or up to $x = 0.15$ [16], and of $Cd_{1-x}Fe_xTe$ up to $x = 0.03$ [17], were measured by x-ray diffraction methods (the bond or the Laue method). These studies showed that the Fe^{2+} atoms substitute for Cd^{2+} atoms, and the lattice parameters decrease linearly with an increase in the iron content, only up to $x = 0.12$ for $Cd_{1-x}Fe_xSe$, and up to $x = 0.01$ for $Cd_{1-x}Fe_xTe$. The extended x-ray absorption fine-structure (EXAFS) technique provides additional information about the displacements of the atoms from their lattice sites [18]. The data of Balzarotti *et al* [19] for $Cd_{1-x}Mn_xTe$ confirm that the different nearest-neighbour Cd–Te and Mn–Te distances are almost independent of x, and that the lattice parameter (cation–cation distance) decreases with an increase in the Mn content. We thus expect that the introduction of Fe atoms into a crystal will lead to the appearance of a local structure (different nearest-neighbour Hg–Se, Cd–Se and Fe–Se as well as Cd–Te and Fe–Te distances) and will influence the valence band electronic structure.

Fundamental reflectivity is a direct method of investigating the electronic band structures of semiconductors, i.e. by probing the transitions between the occupied valence bands and the empty conduction bands. In this context, we have made a comprehensive study of $Hg_{1-x}Fe_xSe$, $Cd_{1-x}Fe_xSe$ and $Cd_{1-x}Fe_xTe$ crystals, in order to

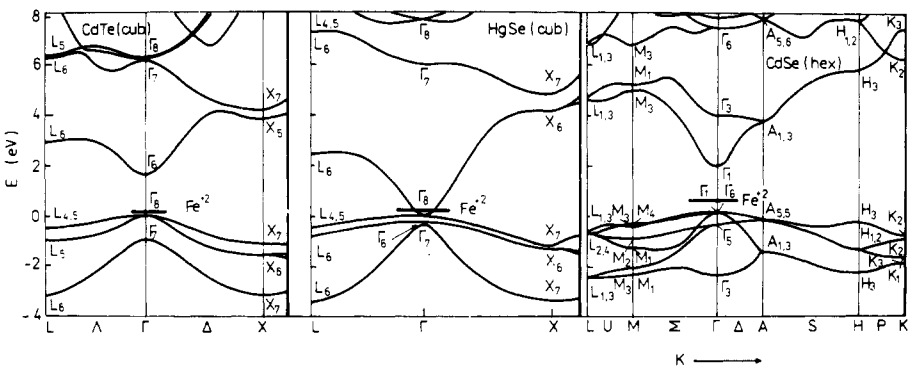

Figure 1. Band structure of $A^{II}_{1-x}Fe_xB^{VI}$ alloys near the Γ point: a wide-gap zincblende (e.g. $Cd_{1-x}Fe_xTe$), narrow-gap zincblende (e.g. $Hg_{1-x}Fe_xSe$) and wurtzite (e.g. $Cd_{1-x}Fe_xSe$).

describe the influence of the Fe ions on the optical properties of these crystals, with an attempt to correlate the change in the Fe content with electronic structure changes. So, we continue and extend the research on the electronic structure of Fe-based SMSCs [20] and present the electronic structure model. As a result, two main effects associated with Fe^{2+} have been observed in the spectra. The first is a significant energy shift of the critical points. The second is the smearing out and a broadening of the characteristic reflectivity maxima with an increase in the Fe content. Section 2 of this paper describes briefly the characterisation of the Fe-based SMSCs and the experimental techniques used in the present investigation. The results of the reflectivity measurements are presented and discussed in section 3. We then, in section 4, discuss the p–d repulsion interaction with the help of a model proposed. Finally, we summarise the results in section 5.

2. Experimental conditions

The single crystals of the SMSCs ($Hg_{1-x}Fe_xSe$, $Cd_{1-x}Fe_xSe$ and $Cd_{1-x}Fe_xTe$) used in this study were grown by a modified Bridgman method at the Institute of Physics, Polish Academy of Sciences. The crystal structures and the composition ranges of the materials studied are summarised in table 1. X-ray diffraction measurements showed that the crystal structure was zincblende for $Hg_{1-x}Fe_xSe$ and $Cd_{1-x}Fe_xTe$, and wurtzite for $Cd_{1-x}Fe_xSe$ (see figure 1). The as-grown crystals are n type. The crystal surfaces were mechanically and chemically polished and cleaned with ethyl alcohol just before the experiment.

The reflectivity spectra obtained for the mixed crystals of $Hg_{1-x}Fe_xSe$ ($0 \leqslant x \leqslant 0.15$), $Cd_{1-x}Fe_xSe$ ($0 \leqslant x \leqslant 0.12$) and $Cd_{1-x}Fe_xTe$ ($0 \leqslant x \leqslant 0.06$), were obtained using unpolarised light. The measurements below 6 eV were carried out, with an SPM-2 monochromator in the infrared, visible and near-ultraviolet ranges. A detailed description of the experimental set-up is available elsewhere [21]. At higher photon energies, a vacuum ultraviolet monochromator (based on the Seya–Namioka scheme) with a flowing-hydrogen low-pressure discharge lamp ($p = 10^{-2}$ Torr), was used as the light source. In the energy range from 5 to 12 eV, the reflectivity spectra were analysed with a resolution of between 5 and 20 meV, respectively. Photomultipliers, with the luminophor (sodium salicylate) deposited on a glass plate, were used as a light detector.

3. Results and discussion

In the measured reflectivity spectra of $Cd_{1-x}Fe_xSe$, $Cd_{1-x}Fe_xTe$ and $Hg_{1-x}Fe_xSe$ crystals, the positions and shapes of the reflectance peaks are of primary importance from the point of view of relating the spectra to the electronic band structures of the

Table 1. The crystal structures of Fe-based II–VI SMSCs.

Alloy	Iron concentration	Structure	Space group
$Cd_{1-x}Fe_xSe$	$0 \leqslant x \leqslant 0.20$	Wurtzite	C_{4v}^6
$Cd_{1-x}Fe_xTe$	$0 \leqslant x \leqslant 0.06$	Zincblende	T_d^2
$Hg_{1-x}Fe_xSe$	$0 \leqslant x \leqslant 0.15$	Zincblende	T_d^2

materials. An analysis of the data is quite difficult because a theoretical explanation of the observed lines would require a calculation of the band structures of these materials. In order to do this, it can be helpful to know the band structures of FeSe and FeTe, which are unknown at present. Therefore, the spectra were explained on the basis of the binary II–VI compound band structures available in the literature. The dependence of the energy position shifts of the main maxima on the Fe concentration will be established. The well known structures are in the notation of Cardona and co-workers [22, 23]: E_0, E_1, $E_1 + \Delta_1$, E_2, E_1', $E_1' + \Delta_1'$. In order to account fully for the optical properties and the influence of the iron concentration on the reflectivity maxima of these alloys, we shall discuss the experimental results for each structure separately.

3.1. $Cd_{1-x}Fe_xSe$

As we stated earlier, $Cd_{1-x}Fe_xSe$ crystals have a hexagonal structure. Cardona and Harbeke [23] show that in a CdSe crystal the direct optical transitions between bands depend on light polarisation. Since most of the structures observed in the spectra obtained by us for unpolarised light are a mixture of the peaks for electric vector parallel and perpendicular to the c axis of the crystal, an analysis of the reflectivity spectra will be complicated. To interpret fully the region of the BZ producing the features in the reflectivity spectra due to allowed transitions, we related the observed structures to the electronic transitions in the CdSe band structure, calculated by Bergstresser and Cohen [24] using the empirical pseudopotential method (EPM).

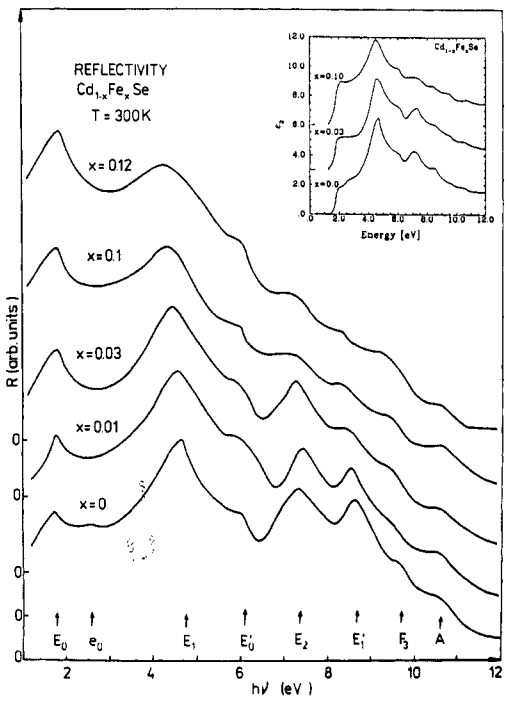

Figure 2. The fundamental reflectivity spectra of $Cd_{1-x}Fe_xSe$ at 300 K versus photon energy from 1 to 12 eV. The inset shows the imaginary part of the dielectric constant ε_2 for three compositions.

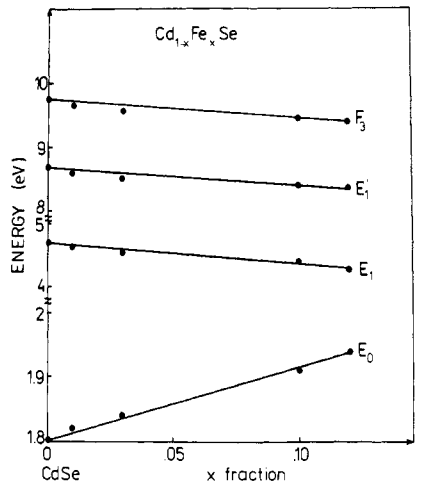

Figure 3. Dependence of the energy positions on composition for $Cd_{1-x}Fe_xSe$.

Figure 2 presents the reflectivity spectra of $Cd_{1-x}Fe_xSe$ ($x = 0, 0.01, 0.03, 0.10$ and 0.12) in the range of energy from 1 to 12 eV, at 300 K. The ε_2 spectra for $Cd_{1-x}Fe_xSe$ are shown as an inset in figure 2, in order to compare them with the experimental reflectivity spectra. As is apparent, the spectra are significantly modified with increasing Fe content. Also, it is clear that, for energies higher than 6 eV, all the features are smeared out for the two Fe concentrations $x = 0.10$ and 0.12. At the same time, the heights of the peaks labelled E_1, E_2 and E_1' decrease, whereas the peak corresponding to the energy gap increases remarkably. The energies of the prominent features in the reflectivity spectra are summarised in table 2. In figure 3, we show the dependence of the maxima position on the iron concentration.

Table 2. The energy positions of the peaks and shoulders discerned in the spectra of $Cd_{1-x}Fe_xSe$, together with their assignment to interband transitions.

Energy (eV) of the reflectivity peaks for the following Fe contents						
$x = 0.0$	$x = 0.01$	$x = 0.03$	$x = 0.10$	$x = 0.12$		Assignment
1.80	1.81	1.84	1.92	1.94	E_0	(Γ_6, Γ_1)–Γ_1 [24]
2.50	—	—	—	—	e_0	(Γ_5–Γ_1) [24]
4.70	4.65	4.55	4.40	4.30	E_1	(U_4–U_3, U_3–U_3, Γ_5–Γ_3) [24]
6.05	6.05	6.05	6.05	6.05	E_0'	(H_3–H_3 and M_2–M_1?) [24]
7.40	7.45	7.35	7.30	7.35	E_2	(K_2–K_2, K_3–K_2) [24]
8.70	8.65	8.50	8.40	8.35	E_1'	(Γ_1–Γ_1, Γ_5–Γ_6, Δ and L) [24]
9.75	9.65	9.55	9.45	9.40	F_3	(region of M and the B face) [24]
10.60	10.55	10.65	10.60	10.50	A	(Valence band–conduction band)

The spectrum for pure CdSe is similar to those seen by other workers [23, 25–27]. The reflectance peak E_0, which occurs at a photon energy of 1.80 eV, is close to the energy of the (Γ_{6v}, Γ_{1v})–Γ_{1c} interband transition [24]. With an increase in Fe content, this peak shifts toward higher energies (0.14 eV) and increases in height with respect to peak E_1 (see figure 2). The shift of the fundamental transition E_0 was found to be almost linear for the Fe concentration range available ($x \leqslant 0.12$), as depicted in figure 3. The variation in the energy gap has already been reported by Arciszewska *et al* [28], using photoionisation absorption and exciton absorption. They performed a survey of E_g for $x \leqslant 0.15$ and confirmed that the change in E_g with x is about 0.15 eV, in agreement with the results reported by us. The weak structure e_0 (see figure 2) at 2.5 eV is attributed to the Γ_{5v}–Γ_{1c} transition (from the next occupied valence band Γ_5 to the first Γ_1 conduction band). It is, as we see, connected with the fundamental energy gap in spite of not being observed with increasing Fe content. Instead, such a peak is seen in the ε_2 spectra for all the contents. The sharp feature E_1 at 4.7 eV is connected with transitions in the vicinity of U and Γ (U_{4v}–U_{3c}, U_{3v}–U_{3c} and Γ_{5v}–Γ_{3c}) in k-space [24]. This maximum is pronounced and even more affected by the iron content. We note that its energy position changes roughly linearly with the Fe content, shifting towards lower energies (by 0.40 eV), through Fe as well as simultaneously becoming increasingly broadened (see figures 2 and 3). The reflectivity maximum E_1', occurring at 8.7 eV, is related to the transitions at Γ (Γ_{1v}–Γ_{1c} and Γ_{5v}–Γ_{6c}), and some contribution of the states from the Δ axis (Γ–A) and

from near the L point of the BZ may be expected [24]. As shown in figures 2 and 3, this structure broadens and shifts towards lower energies (0.35 eV) with an increasing amount of iron.

The weak structure E_0' at 6.05 eV was ascribed to the transitions H_{3v}–H_{3c} and M_{2v}–M_{1c} [24]. As may be seen in figure 2, this peak does not depend on iron concentration; hence, we interpret it as a CdSe-related transition. The E_2 feature at 7.4 eV corresponds to the transitions at K (K_{2v}–K_{2c} and K_{3v}–K_{2c} [24]. This peak does not shift noticeably with increasing x but becomes rapidly broadened with increasing Fe concentration (see figure 2). In contast, the ε_2 spectra show that this peak shifts to higher energies, by about 0.15 eV [20]. The F_3 shoulder at 9.75 eV was ascribed to transitions in the region of the M and B face of the BZ [24]. This structure shifts to lower energies (0.35 eV) upon increasing the amount of Fe. Finally, the energy at which the A structure occurs is not sensitive to the Cd 4d band transitions as was suggested previously [23] and seems to be due to the transitions between the valence and conduction bands. As depicted in figure 2, this feature is not affected by changes in Fe composition.

To understand the experimental data, we should note that in $A^{II}B^{VI}$ compounds the valence band close to the Γ point (2–3 eV) results mostly from the p-like states of the group VI atom, while in the other parts of the valence band a contribution of the s-like states of the group II atom hybridised with the p-like states of the group VI atom appears [29, 30]. The lowest conduction band is built up of the s-like electrons of the cation (group II). In mixed crystals, Fe (configuration $3d^64s^2$) substitutes for the group II element. The two 4s electrons of Fe, together with the two electrons of the group II atom, create the conduction band. Upon increasing the amount of Fe, there is a larger admixture from the Fe 4s states in comparison with the s states of the group II element. Also, occupied and unoccupied Fe 3d states appear at random. Hence, it is reasonable to search for an explanation for the changes in the electronic structure in the crystals in the presence of the Fe 3d and Fe 4s states.

The shift of E_0 is about +0.14 eV when x increases from 0 to 0.12, while the shifts of E_1 and E_1' were found to be −0.40 eV and −0.35 eV, respectively. This suggests that the minimum of the conduction band Γ_{1c} (E_0) rises with increasing Fe content, while the second-lowest conduction band Γ_{3c} (E_1) moves to lower energies. This effect may be explained in terms of the above picture, as caused by the larger admixture of the 4s states of Fe, compared with Cd 5s. Similar interpretations were reported by Taniguchi *et al* [31] and Lautenschlager *et al* [32] for $Cd_{1-x}Mn_xFe$. The shift of E_1' is connected with the change in the (Γ_{6c}, Γ_{1c}) states. These final states are located about 7–8 eV above the valence band maximum (VBM). This may be taken as evidence for the existence and influence of the Fe 3d empty states on the conduction band. On the other hand, the Γ_{5v} valence band which takes part in the e_0, E_1 and E_1' transitions should be repelled to higher energies with increasing x by interaction with the Fe 3d states, whereas the VBM (Γ_{6v}, Γ_{1v}) remains nearly the same, owing to the large cation Se 4p contribution to these states, as suggested by Lautenschlager *et al* [32]. From the point of view of photoemission [33], there are two additional features in the valence band region, at about 3.6 and 0.5 eV. The second feature occurring near the top of the VBM (Γ) supports our suggestion that there exists an interaction of the electrons in the valence band close to the Γ point of the BZ with the 3d electrons of Fe. This is consistent with the results reported by Kisiel *et al* [34] for these materials. These workers arrive at the conclusion that the band structure is influenced more by the Fe 3d states at Γ and the high-symmetry directions than in the volume or at the edges of the BZ. Also they indicate the presence of a strong interaction between the Fe 3d and Se 4p states. Following Kisiel *et al* [34], we attribute

the above modification to hybridisation of the top valence band Se 4p with the 3d states of Fe.

The situation for the E_2 structure is different. The transitions ascribed to the K point show a behaviour which is opposite to that characterising the transitions at the centre of the BZ. This structure is likely to be strongly affected by the presence of the Fe ions. This effect suggests that in Fe alloys the final K_{2c} and K_{3c} states in the conduction band are degenerate with empty spin-down Fe 3d states. These states (K_{2c} and K_{3c}) are located at 6–8 eV above the VBM, like the Γ_{6c} and Γ_{1c} states. As a consequence, this enables us to locate the empty 3d states of Fe somewhere in between the first (lower part) and second (upper part) conduction band. Also, our assignment agrees well with that reported for $Cd_{1-x}Mn_xTe$ [35]. Of course, the above modifications are not discussed by Kisiel *et al* [34]. Another problem is that, at even high energies, the F_3 structure is connected strongly with the empty Fe 3d states. Moreover, this behaviour is somewhat like that observed for the K and Γ final states. However, we have been careful to locate it at the same distance above the maximum valence band edge as that of the Γ and K final states.

3.2. $Cd_{1-x}Fe_xTe$

Figure 4 shows the measured room-temperature reflectivity in $Cd_{1-x}Fe_xTe$ (x = 0, 0.02, 0.03 and 0.06) crystals in the energy range from 1 to 12 eV along with the ε_2 spectra as an inset. Considerable structure is apparent in all the curves and, as expected, there is reasonably close correspondence in the positions and shapes of the peaks. The positions of all the experimental reflectivity peaks are summarised in table 3.

The reflectivity features seen by us in pure CdTe agree in both energy position and

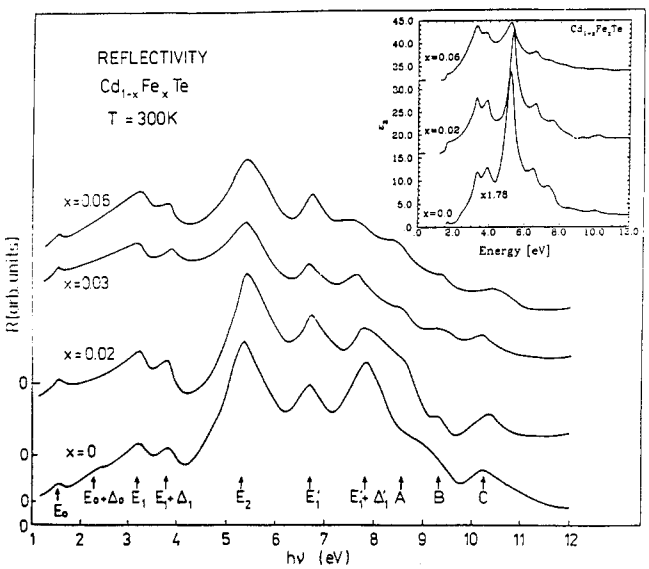

Figure 4. Room-temperature reflectivity spectra of $Cd_{1-x}Fe_xTe$ crystals versus photon energy for different values of x. The inset shows the imaginary part of the dielectric constant ε_2 for three compositions. The CdTe spectrum was multiplied by 1.78 to obtain the same height of the E_1 peak for all the crystals.

Table 3. The energies of prominent features for $Cd_{1-x}Fe_xTe$, together with identification of the interband transition.

Energy (eV) of the reflectivity peaks for the following Fe contents					
$x = 0.0$	$x = 0.02$	$x = 0.03$	$x = 0.06$		Assignment
1.55	1.55	1.55	1.55	E_0	(Γ_8–Γ_6) [37]
2.40	—	—	—	$E_0 + \Delta_0$	(Γ_7–Γ_6)
3.22	3.25	3.20	3.25	E_1	($L_{4,5}$–L_6 [37]; Λ (0.43, 0.43, 0.43) [36])
3.85	3.85	3.88	3.85	$E_1 + \Delta_1$	(L_6–L_6 [37]; Λ (0.43, 0.43, 0.43) [36])
5.35	5.40	5.40	5.40	E_2	(Δ_5–Δ_5 (0.5, 0, 0), (0.75, 0.25, 0.25), Δ_5–Δ_5 (0.75, 0, 0) [37]; Δ (0.7, 0, 0), (0.9, 0.2, 0.2), Σ (0.7, 0.7, 0), Δ (0.7, 0, 0), (0.35, 0.07, 0.7), Δ (0.2, 0, 0) [36])
6.70	6.70	6.68	6.75	E_1'	($L_{4,5}$–L_6 [37]; (0.6, 0.5, 0.2) [36])
7.80	7.73	7.65	7.60	$E_1 + \Delta_1'$	(L_6–$L_{4,5}$ [37]; (0.6, 0.2, 0.1) [36])
—	8.70	8.60	8.50	A	} Valence band–conduction band
9.10	9.35	9.35	9.35	B	
10.20	10.35	10.35	10.00	C	
0.85	—	—	—	Δ_0	
0.63	0.58	0.68	0.60	Δ_1	
1.10	1.03	0.97	0.85	Δ_1'	

shape with the results published previously [22, 36, 37]. The E_0 ($\boldsymbol{k} = \mathbf{0}$) peak corresponds to the Te 5p → Cd 5s interband transition at Γ, while $E_0 + \Delta_0$ is its spin–orbit split component. The spin–orbit splitting of the valence band at Γ is $\Delta_0 = 0.85$ eV, in good agreement with the corresponding value found in the literature [35, 36]. The (E_1, $E_1 + \Delta_1$) and (E_1', $E_1' + \Delta_1'$) structures represent transitions from the spin–orbit split valence bands in the vicinity of the L point along the Λ direction $\langle 111 \rangle$ of the BZ, to the lowest and second-lowest conduction bands. These transitions have the same initial states [36, 37]. The $\Delta_1 = 0.63$ eV shown in table 3 agrees well with two-thirds of the estimated $\boldsymbol{k} = \mathbf{0}$ splitting. $\Delta_1' = 1.10$ eV is the sum of Δ_1 and the spin–orbit splitting of the final states Δ_c of the second-lowest conduction band. This value is much larger than the values found in the literature [22, 35, 38]. The well pronounced E_2 feature represents a transition poorly localised in $\boldsymbol{k}$-space, in particular, in the large part of the volume along the Δ and Σ directions [27, 37]. Finally, the shoulders labelled B and C seem to be due to some transitions between the valence and conduction bands.

Generally, the presence of Fe ions (see figure 4) gives

(i) almost no change in positions of some of the peaks (E_0, E_1, $E_1 + \Delta_1$, E_1', B and C) and, hence, it is easy to interpret them as due to interband transitions in pure CdTe (see table 3),

(ii) a remarkable broadening of the reflectivity peaks obtained in the range of energy $h\nu$ between 4 and 9 eV,

(iii) a decrease and shift in the $E_1' + \Delta_1'$ peak to lower energy,

(iv) an appearance of a shoulder labelled A, not observed in a CdTe spectrum.

The disappearance of the $E_0 + \Delta_0$ shoulder and the slight increase in the E_0, E_1 and $E_1 + \Delta_1$ peak heights with respect to the E_2 peak, as well as the decrease in the $E_1 + \Delta_1$ peak height with respect to the E_1 peak, without any change in their positions, testify to

the introduction of a small admixture of Fe states to the band structure of CdTe. As shown in table 3, the energy gap E_0 is constant for the range of x values considered. These results are unlike those reported by Joshi and Mogollón [39] concerning the optical absorption edge of $Cd_{1-x}Fe_xTe$ (x up to 0.05) crystals. They showed that the region close to the absorption edge is dominated by the Fe^{2+} states, and that the fundamental gap moves slightly towards lower energies. We also note that photoemission studies [33] yield information about the two well established features (0.6 and 3.6 eV) in the valence band region. The first feature, occurring close to the Γ point of the BZ agrees well with our suggestion that there exists mutual influence of the electrons in the valence band close to Γ with the d electrons of Fe. On the other hand, because of the solubility limit we cannot find out whether the maxima are affected by replacement of the Cd 5s states by Fe 4s in the conduction band. The E_2 structure, outside the high-symmetry points along the Δ (Γ–X) and Σ (Γ–K) directions of the BZ, broadens slightly with increasing Fe content, while its height strongly decreases. This modification is observed in the reflectivity spectra as well as in ε_2. Similar behaviour has been found for the nonmagnetic $Cd_{1-x}Zn_xTe$ system [38, 40]. However, there undoubtedly exists a strong Fe 3d admixture in the volume, near-degenerate with the states along the Δ and Σ directions.

The main discernible changes in the electronic structure which are introduced by iron occur for some of the states at the L point (the shifted $E_1' + \Delta_1'$ peak agrees with the L_6–$L_{4,5}$ transition; the $\boldsymbol{k}$-vector at the L point corresponds to the main $\langle 111 \rangle$ direction of Cd–Te bonding). The decrease of $\Delta_1' = \Delta_1 + \Delta_c$, as presented in table 3, is about 0.25 eV, as x goes from 0 to 0.06. Since Δ_1 is constant, the quantity that decreases is the spin–orbit splitting Δ_c. Hence, we expect strong modifications of the final states. These states are located about 6–7 eV above the valence band edge. This suggests that the empty 3d states of Fe will be located between the lowest and second-lowest conduction band, in agreement with the results reported by Kisiel *et al* [35] for $Cd_{1-x}Mn_xTe$, as well as those reported for $Cd_{1-x}Fe_xSe$ in this section.

A peculiar feature of the spectra is the additional shoulder A, which appears in the presence of Fe atoms, as shown in figure 4. With increasing x, peak A shifts to lower energies (0.20 eV). It may result from a splitting of shoulder B into two components. Therefore, the precise nature of these transitions remains unexplained.

3.3. $Hg_{1-x}Fe_xSe$

It is well established that HgSe is a so-called inverted band-structure semiconductor [41, 42]. The conduction and valence bands are degenerate at the centre of the BZ ($E_g < 0$) with the Γ_8 p-like symmetry state above the Γ_6 s-like symmetry state. The energy band structure of HgSe has been calculated by Bloom and Bergstresser [43] using the EPM, and by Overhof [44] using the relativistic Green function (the KKR method). In the following, we relate our experimental data to the electronic transitions in the HgSe band structure.

The reflectivity spectra of cubic $Hg_{1-x}Fe_xSe$ ($x = 0$, 0.02, 0.05, 0.10 and 0.15) over the energy range of 1–12 eV at room temperature are shown in figure 5. It is clear that there are some peaks which are independent of composition, particularly those at high energies. The main results obtained in this study are displayed in table 4, which shows the energies and interband transitions associated with the prominent optical structures in HgSe.

Good agreement is found between the curve for HgSe, obtained by us, and that

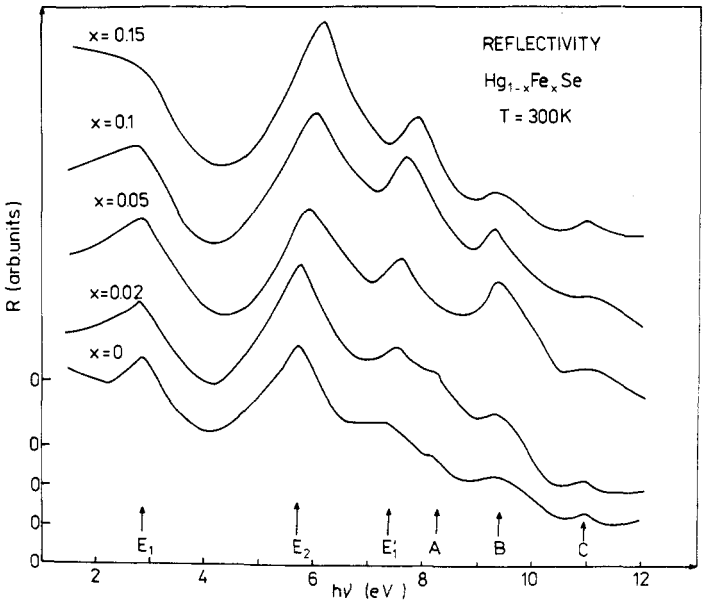

Figure 5. The reflectivity spectra of $Hg_{1-x}Fe_xSe$ at room temperature versus energy.

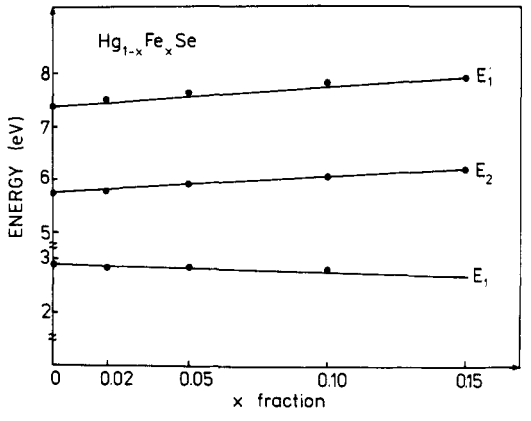

Figure 6. Positions of the shifted maxima in the spectra of $Hg_{1-x}Fe_xSe$ versus composition.

shown by Scouler and Wright [45]. The main structure E_1, at 2.90 eV, has been assigned to the $L_{4,5v}$–L_{6c} transition [43, 44]. Upon substitution of Hg by Fe, this peak broadens and shifts to lower energies (0.02 eV) with increasing x. The considerable broadening, as shown in figure 5, suggests that there exists an influence of Fe at the L point, as well as along the Λ direction of the BZ. The second main reflectivity peak (E_2) at 5.75 eV, has been ascribed to transitions at the X point of the BZ [43], probably the transitions from the valence band X_6 or X_7 to the X_{7c} conduction band level (the second-lowest conduction band). This structure shifts to higher energies (0.45 eV) as the amount of iron increases. At the same time, its height increases with respect to the E_1 peak. The E_1' feature at 7.35 eV is attributed to the $L_{4,5v}$–L_{6c} transitions [43], in contrast with the assignment reported by Overhof [44], who ascribes it to the W_{6v}–W_{6c} transitions, out of high-symmetry points. With increasing x (see figure 5), this peak strongly shifts to higher

Table 4. The energies and interband transitions associated with prominent optical structure in $Hg_{1-x}Fe_xSe$.

Energy (eV) of the peaks for the following Fe contents						
$x = 0.0$	$x = 0.02$	$x = 0.05$	$x = 0.10$	$x = 0.15$		Assignment
2.90	2.87	2.85	2.80	2.70	E_1	($L_{4,5}$–L_6 [43, 44])
5.75	5.80	5.90	6.05	6.20	E_2	at X point of BZ [43]
7.35	7.50	7.60	7.80	7.90	E_1'	($L_{4,5}$–L_6 [43] W_6–W_6 [44])
8.25	8.25	—	—	—	A	($L_{4,5}$–$L_{4,5}$ [43] $L_{4,5}$–L_6 [44])
9.35	9.30	9.35	9.3	9.35	B	(L_6(first valence band)–L_6 (third conductance band) [44])
11	11	11.1	11	11	C	(L_6(second valence band)–L_6 (third conduction band) [44])

energies (0.55 eV), simultaneously becoming sharper. The weak A structure at 8.25 eV is attributed to $L_{4,5v}$–$L_{4,5c}$ [43] and $L_{4,5v}$–L_{6c} [44] transitions. It is (see figure 5) only visible for HgSe and $Hg_{0.98}Fe_{0.02}Se$. Finally, the reflectivity peaks B and C at 9.3 and 11 eV, respectively (see table 4) are caused by transitions at the L point of the BZ [44], and not by atomic d-band excitation as suggested by Scouler and Wright [45]. As can be seen in figure 5, they are not affected by the presence of Fe ions; hence, we interpret them as HgSe-related transitions.

Figure 6 shows the energies of E_1, E_2 and E_1', as a function of x. In all cases, the results show a linear dependence of the gaps on composition. As for the energy gap E_0, due to the Γ_6–Γ_8 direct transition, it is too weak to be seen in the reflectivity spectrum. In spite of that, there is a contribution of the Fe states to the Γ states. Hence, one can also expect that the band gap opens up [46]. This, however, has not yet been experimentally established. The considerable d admixture in the upper valence region (at Γ) has also been confirmed by photoemission measurements and detailed cross-section studies [47, 48]. They showed two additional features, at about 3.5 and 0.2–0.3 eV below the valence band maximum, in the valence band region. The second feature was related to hybrid p–d orbitals close to Γ.

The E_1, E_1' and A features represent transitions in the vicinity of the L point and/or in the Λ direction $\langle 111 \rangle$ of the BZ, to the lowest, second and third conduction bands. These structures are strongly influenced by Fe ions. As may be seen in figure 6, the energy of E_1 decreases with increasing x, whereas the energy of E_1' strongly increases. On the other hand (see figure 5), the A feature disappears for higher concentrations. Also, it is clear from table 4 that these transitions have the same intial state $L_{4,5v}$. The $L_{4,5v}$ upper valence band region remains roughly stationary. In contrast, the L_{6c} conduction band minimum decreases, owing to the large cation s contribution to this state (a 4s admixture of Fe, as compared with Hg 6s). In the region where the A structure disappears, strong disorder due to the presence of the Fe states manifests itself. The L_{6c} state energy increases by about 0.55 eV, and it may overlap the $L_{4,5c}$ state. These states ($L_{4,5c}$ and L_{6c}) are located at about 7–8 eV above the VBM. Hence, the practical disappearance and the strong shift in the upper conduction band region ($L_{4,5c}$ and L_{6c}) result mainly from the hybridisation of the L final states with the unoccupied Fe 3d states. This effect suggests that the lowest and second-lowest conduction bands are pushed apart from each other by the empty Fe 3d states, which should be placed between

them. Our assignment agrees well with that depicted in this section for $Cd_{1-x}Fe_xSe$ and $Cd_{1-x}Fe_xTe$.

The E_2 structure, as mentioned above, corresponds to transitions from the upper valence band region at X to the second-lowest conduction band X_{7c}. As can be seen in figure 6, this peak shifts strongly towards higher energies as x increases. This state is located at about 6 eV above the VBM. This behaviour is, to some extent, like that of the L final states, i.e. hybridisation of the L states with the empty Fe 3d states.

4. A model of p–d hybridisation in Fe-based SMSCs

In a tetrahedral crystal field, the transition-metal d states are split into a doublet e and a triplet t_2. The e states are lower in energy than the t_2 states. An Fe atom has a $3d^64s^2$ configuration and, according to Hund's rule, only five spin-up electrons may occupy the e_+^2 and t_+^3 ground state; the last spin-down electron must be located in the e_-^1 state. The physical and magnetic properties of $A^{II}_{1-x}Fe_xB^{VI}$-type SMSCs are mainly connected with the position of the Fe^{2+} ground state with respect to the conduction band, as well as the positions of the energy levels themselves. The absorption [28], transport [6, 8] and surface photovoltage spectroscopy [13] measurements yield important information on the position of the Fe^{2+} $3d^6$ level in the band structures of the $A^{II}_{1-x}Fe_xB^{VI}$ alloys. These experiments determine precisely the location of the Fe^{2+} states and found them to lie for the different structures either in the band gap or in the conduction band, but in both cases over the edge of the valence band (see figure 1). On the other hand, photoemission studies [7, 33, 47, 48] indicate two constant features in the valence band region. Our interpretation of the optical properties of these materials suggests that the feature in the vicinity of the top of the valence band (0.6 eV for wide gap, and 0.2–0.3 eV for zero gap) occur owing to the hybridisation with the p states. Therefore, we locate the last spin-down $d_\downarrow$ electron over the top of the valence band. This agrees well with the results of Kisiel *et al* [34], who place the same states in the energy gap.

Figure 7 shows a schematic diagram of the p–d-coupling mechanism for a zincblende $A^{II}_{1-x}Fe_{1-x}B^{VI}$ wide-gap alloy. The energy levels presented in the figure originate from photoemission, transport and absorption measurements [7, 33, 47, 48]. The spin-up $d_\uparrow$ and spin-down $d_\downarrow$ states are degenerate with the sp valence and conduction bands,

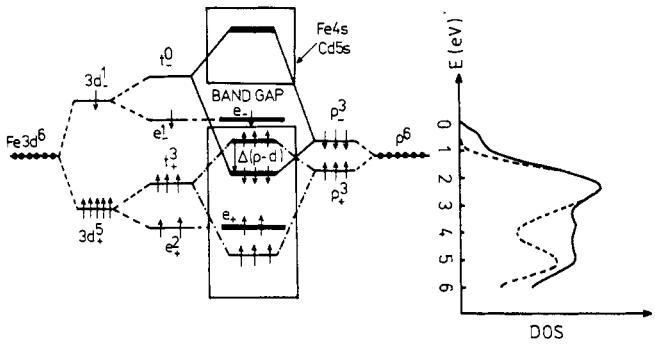

Figure 7. A schematic energy diagram of p–d coupling for an $A^{II}_{1-x}Fe_xB^{VI}$ wide-gap zincblende SMSC. On the right-hand side, the EDC of the valence band for $Cd_{1-x}Fe_xSe$ (——) and for CdSe (– – –) are presented.

respectively. The s–d effect is not shown in the left-hand side of figure 7. The upper valence band anion p states have $t_2(\Gamma_{15})$ symmetry. Instead, for 3d states, the e states have Γ_{12} symmetry at $\boldsymbol{k} = \mathbf{0}$, and t_2 states have Γ_{15} symmetry. The former do not hybridise in a tetrahedral environment with the p states since the matrix element of the Fe 3d e states and the p states is zero. Therefore, we ascribe them to e state symmetry, as depicted in figure 7. On the other hand, the Fe $4s^2$ electrons as well as the s(Cd, Hg) electrons, create bonding and antibonding states with the p electrons in the valence and conduction bands, respectively [49]. Moreover, the interaction between the Γ_{15}(p) state and the cation Γ_{15}(d) spin-up state of t_2 symmetry yields lower bonding and higher antibonding states in the valence band [50]. This, in turn, leads to strong mixing with the upper valence region p states, i.e. the p–d-coupling matrix elements. The Γ_1 conduction band minimum is, for symmetry reasons, unaffected by hybridisation. In figure 7, we also present the EDC of the valence band for $Cd_{1-x}Fe_xSe$ alloys (right-hand side) [33], along with occupied and unoccupied atomic states forming the valence and conduction bands (left-hand side). It is clear that these emphasise the changes in the electron density of states of the mixed-crystal valence band, and the contribution of the Fe 3d electrons to this band.

While the position of the Fe 3d state is closer to the band extrema, the symmetry allows the interaction, and one can expect more hybridisation. This, in turn, leads to an increase in the exchange constants J_{dd} [1–3]. The exchange constant $N_0\alpha > 0$ and $N_0\beta < 0$ correspond to sp–d exchange interactions for electrons and holes, respectively. Note that in wide-gap SMSCs the exchange integral $N_0\alpha$ refers to the lowest conduction band (s like at the Γ point), whereas the $N_0\beta$ constant applies to the upper valence band (p like at the Γ point). On the other hand, in a zero-gap situation, the conduction electrons are described only by $N_0\beta$ [5, 51]. As was stated earlier, the exchange constant J_{dd} has been measured and found to be antiferromagnetic for the nearest neighbours for $Cd_{1-x}Fe_xSe$, $Hg_{1-x}Fe_xSe$ and $Zn_{1-x}Fe_xSe$ alloys [9–11]. This means that there exists hybridisation of the $3d^6$ level with the p-band electrons. Recently, Heiman *et al* [52] have estimated the magnitude of $N_0\alpha$ (0.23 eV) for $Cd_{1-x}Fe_xSe$. Moreover Twardowski *et al* [53] have found it to be equal to 0.22 eV for $Zn_{1-x}Fe_xSe$. On the other hand, for a zero-gap SMSC such as $Hg_{1-x}Fe_xTe$, $N_0\beta$ equal to 1.6 eV was reported by Serre *et al* [54]. The above observations lead, in all cases, to the sp–d exchange interaction and are generally in agreement with the situation for the well known Mn-based SMSCs [5, 55]. These facts underline the connection between the sp–d hybridisation and the band structure of the materials as well as showing how strongly are the exchange constants and the magnetic properties connected with the energy band structure.

5. Summary and conclusion

In this paper, we presented results of a comprehensive study of the optical properties of representative Fe-based SMSCs $Cd_{1-x}Fe_xSe$, $Cd_{1-x}Fe_xTe$ and $Hg_{1-x}Fe_xSe$. It follows from our results that there exists discernible change in the shapes of the valence and conduction bands, caused by the disorder occurring in the lattice. In spite of that, the band structure of these alloys resembles closely that of the $A^{II}B^{VI}$ materials [56].

The common feature in the reflectivity spectra of the SMSCs investigated is the broadening of the reflectivity peaks with increasing iron concentration. This effect is connected with the shape of the crystal potential, resulting from the absence of long-

range order in the crystal. This conclusion was arrived at by Kendelewicz [57] for $Cd_{1-x}Mn_xTe$.

The increase in x strongly influences the optical transitions at the low- and high-symmetry points. For $Cd_{1-x}Fe_xSe$ and $Hg_{1-x}Fe_xSe$, the band structure at the centre ($\boldsymbol{k} = \mathbf{0}$) is influenced more strongly by Fe ions than for a $Cd_{1-x}Fe_xTe$ alloy, whereas at the other high-symmetry points all the materials are affected by Fe content. The last feature suggests that the influence of the Fe electrons on the conduction bands modifies the structure of the final states involved in some of the optical transitions observed. This allows us to locate the approximate position of the empty Fe 3d states somewhere in between the lowest and second-lowest conduction bands, at an energy of about 6–7 eV above the valence band edge. On the other hand, for the valence band, the exchange interaction implies strong hybridisation of the Fe state with the valence band and/or different location of the Fe state in the valence band, i.e. p–d hybridisation.

When the results of theoretical calculations of the band structure of $A^{II}_{1-x}Fe_xB^{VI}$ becomes available, precise interpretation of the role of the Fe 3d electrons in the electronic structure of the alloy will be possible, since the experimental data alone do not account for the band structure (p–d hybridisation).

Acknowledgments

The authors are grateful to Dr A Mycielski for supplying the samples and to Dr K Leśniak for careful reading of the manuscript. This work was supported by programmes CPBP 01.04 and CPBP 01.08.

References

[1] Gałązka R R 1982 *Proc. Int. Conf. on Narrow Gap Semiconductors, Lecture Notes in Physics 152* (Berlin: Springer) 294; 1985 *J. Cryst. Growth* **72** 364; 1986 *Proc. 18th Inst. Conf. on the Physics of Semiconductors (Stockholm, 1986)* ed O Engström (Singapore: World Scientific) p 1727
[2] Brandt N B and Moschalkov V V 1984 *Adv. Phys.* **33** 193
[3] Gaj J A 1980 *J. Phys. Soc. Japan Suppl.* A **49** 797
[4] Giriat W and Furdyna J K 1988 *Semicond. Semimet.* **25** 1
[5] Furdyna J K 1988 *J. Appl. Phys.* **64** R29
[6] Mycielski A, Dzwonkowski P, Kowalski B J, Orłowski B A, Dobrowolska M, Arciszewska M, Dobrowolski W and Baranowski J M 1986 *J. Phys. C: Solid State Phys.* **19** 3605
[7] Orłowski B A, Kowalski B J and Chab V 1989 *Proc. 9th Int. Conf. on Vacuum Ultraviolet Radiation Physics (Honolulu, HI 1989)* to appear in *Phys. Scr.*
[8] Mycielski A 1988 *J. Appl. Phys.* **63** 3279
[9] Twardowski A 1989 *Acta Phys. Pol.* A **75** 327
[10] Lewicki A, Mycielski A and Spałek J 1986 *Acta Phys. Pol.* A **69** 989
[11] Lewicki A, Spałek J and Mycielski A 1987 *J. Phys. C: Solid State Phys.* **20** 2005
[12] Petrou A, Liu X, Waytena C, Warnock J and Giriat W 1987 *Solid State Commun.* **61** 767
[13] Sarem A, Kuźmiński S and Orłowski B A 1990 *Proc. 19th Int. School on Physics of Semiconductors (Jaszowiec, 1990)* to appear in *Acta. Phys. Pol.*
[14] Orłowski B A, Kowalski B J, Sarem A, Mycielski A, Velicky B and Chab V 1988 *Proc. 19th Int. Conf. on the Physics of Semiconductors (Warsaw, 15–18 August 1988)* vol 2 (Warsaw: Poland) p 1267
[15] Sarem A, Jezierski K, Kowalski B J, Bąk-Misiuk J, Misiewicz J, Orłowski B A and Mycielski A 1989 *Acta Phys. Pol.* A **75** 67
[16] Smith K, Marsella J, Kershaw R, Dwight K and Wold A 1988 *Mater. Res. Bull.* **23** 1423
[17] Sarem A, Kowalski B J, Majewski J, Górecka J, Orłowski B A, Mycielski A and Jezierski K 1990 *Acta Phys. Pol.* A **77** 407

[18] Mikkelsen J C and Boyce J B 1983 *Phys. Rev.* B **28** 7130
[19] Balzarotti A, Czyzyk M, Kisiel A, Motta N, Podgorny M and Zimnal-Starnowska M 1984 *Phys. Rev.* B **4** 2295
[20] Kowalski B J, Sarem A and Orłowski B A 1990 *Phys. Rev.* B submitted
A Kramers–Kronig analysis of the reflectivity data was performed for pure CdSe and CdTe, for two compositions of $Cd_{1-x}Fe_xSe$ ($x = 0.03$, 0.10) and $Cd_{1-x}Fe_xTe$ ($x = 0.02$, 0.06), and the relationships between the optical constants of the alloys with different Fe contents were established. It was found that the observed dependence of the position and intensities of the spectral peaks on the Fe content allows us to estimate the contribution of Fe-derived states to the band structures of the crystals investigated.
[21] Becla P, Gumienny Z and Misiewcz J 1979 *Opt. Appl.* **9** 144
[22] Cardona M and Greenaway D L 1963 *Phys. Rev.* **131** 98
[23] Cardona M and Harbeke G 1965 *Phys. Rev.* **137** A1467
[24] Bergstresser T K and Cohen M L 1967 *Phys. Rev.* **164** 1069
[25] Cardona M 1963 *Phys. Rev.* **129** 1068
[26] Balkanski M and Petroff Y 1964 *Proc. 7th Int. Conf. on Semiconductors* (Paris: Dunod) p 245
[27] Freeouf J L 1973 *Phys. Rev.* B **7** 3810
[28] Arciszewska M, Mycielski A, Dobrowolska M, Dobrowolski W, Baranowski J M, Warmiński T, Witkowska B and Blinowska U 1986 *Acta Phys. Pol.* A **69** 989
[29] Kobayasi A, Sankey O F, Volz S H and Dow J D 1983 *Phys. Rev.* B **28** 935
[30] Orłowski B A 1976 *Postepy Fiz.* **27** 463
[31] Taniguchi M, Ley L, Johnson R L, Ghijsen J and Cardona M 1986 *Phys. Rev.* B **33** 1206
[32] Lautenschlager P, Logothetidis S, Viña L and Cardona M 1985 *Phys. Rev.* B **32** 3811
[33] Orłowski B A, Kowalski B J and Sarem A 1990 unpublished
Orłowski B A, Fraxedas J, Denecke R, Kowalski B J, Mycielski A and Ley L 1990 *Proc. 19th Int. School on the Physics of Semiconductors Comp (Jaszowiec 1990)* to appear in *Acta. Phys. Pol.*
[34] Kisiel A, Piacentini M, Antonangeli F, Zema N and Mycielski A 1989 *Solid State Commun.* **70** 693
[35] Kisiel A, Piacentini M, Antonangeli F, Oleszkiewicz J, Rodzik A, Zema N and Mycielski A 1987 *J. Phys. C: Solid State Phys.* **20** 5601
[36] Chadi D J, Walter J P, Cohen M L, Petroff Y and Balkański M 1972 *Phys. Rev.* B **5** 3058
[37] Chelikowsky J R and Cohen M L 1976 *Phys. Rev.* B **14** 556
[38] Sobolev V V, Maksimova O G and Kroitoru S G 1981 *Phys. Status Solidi* b **103** 499
[39] Joshi N V and Mogollón L 1985 *Prog. Cryst. Growth Characteristics* **10** 65
[40] Saito K, Ebina A and Takahashi T 1972 *Solid State Commun.* **11** 841
[41] Broerman J G 1969 *Phys. Rev.* **183** 754
[42] Harman T C 1967 *Physics and Chemistry of II–VI Compounds* ed M Aven and J S Prener (Amsterdam: North-Holland) ch 15
[43] Bloom S and Bergstresser T K 1970 *Phys. Status Solidi* **42** 191
[44] Overhof H 1971 *Phys. Status Solidi* b **43** 221
[45] Scouler J W and Wright G B 1964 *Phys. Rev.* **133** A736
[46] Mycielski A private communication
[47] Wall A, Caprile C, Franciosi A, Vaziri M, Reiferberger R and Furdyna J K 1986 *J. Vac. Sci. Technol.* A **4** 2010
[48] Dzwonkowski P, Kowalski B J, Orłowski B A and Mycielski A 1986 *Acta Phys. Pol.* A **69** 1047
Kowalski B J, Chab V, Orłowski B A, Majewski J, Sarem A and Mycielski A 1988 *Acta Phys. Pol.* A **73** 455
[49] Phillips J C 1973 *Bonds and Bands in Semiconductors* (New York: Academic)
[50] Wei S-H and Zunger A 1986 *Phys. Rev. Lett.* **56** 2391; 1987 *Phys. Rev.* B **35** 2340
Jaffe J E and Zunger A 1984 *Phys. Rev.* B **29** 1882
[51] Bhattacharjee A K, Fishman G and Coqblin B 1983 *Physica* B **117–118** 449
[52] Heiman D, Petru A, Bloom S H, Shapira Y, Isaacs E D and Giriat W 1988 *Phys. Rev. Lett.* **60** 1876
[53] Twardowski A, Swagten H J M, d Wertering T F H V and de Jonge W J M 1987 *Solid State Commun.* **64** 63
[54] Serre H, Bastard G, Rigaux C, Mycielski J and Furdyna J K 1982 *Proc. 4th Int. Conf. on the Physics Narrow Gap Semiconductors* ed E Gornik (Berlin: Springer) p 321
[55] Oseroff S and Keesom P H 1988 *Semicond. Semimet.* **25** 91
[56] Reiferberger R and Kossut J 1987 *J. Vac. Sci. Technol.* A **5** 2995
[57] Kendelewicz T 1981 *J. Phys. C: Solid State Phys.* **14** L407